# Effects of Pressure and Supercritical Fluids on the Viscosity of Polyethylene

**Hee Eon Park† and John M. Dealy***

*Department of Chemical Engineering, McGill University, 3610 University Street, Montreal, Quebec, Canada H3A 2B2*

*Received April 1, 2006; Revised Manuscript Received May 29, 2006*

ABSTRACT: A high-pressure sliding plate rheometer was used to determine the effects of supercritical fluids and pressure on the viscosity of molten high-density polyethylene (HDPE). In this instrument, the shear strain, temperature, pressure, and gas concentration are all uniform, and a shear stress transducer senses the stress in the center of the sample to eliminate edge effects. The effect of pressure alone at 180 °C was determined up to 70 MPa. The sample exhibited piezorheologically simple behavior, and the Barus equation was found to describe the pressure-shift factor. The effects of gas concentration and pressure on the viscosity were determined up to 23 wt % $CO_2$ concentration and 34.5 MPa. Because the gas of interest is the pressurizing fluid, it is necessary to ensure that the sample was saturated before measurements were made. The saturation time was estimated by use of Fick's law, and the prediction was confirmed by monitoring the viscosity as a function of time. This implies that the rheometer can be used to obtain a good estimate of the diffusion coefficient for gas into polymer. Small-amplitude oscillatory shear was found to significantly accelerate the diffusion process. To interpret the data, it was necessary to determine the pressure−volume−temperature behavior of pure HDPE, and the Tait model provided a good fit to the data. The solubility of gas and the swollen volume of polymer were also required, and these were determined using a magnetic suspension balance. The Sanchez−Lacombe model was used to analyze these data. Using both horizontal and vertical shift factors for concentration and a horizontal shift factor for pressure led to an excellent superposition of all data. The shift factor for concentration alone was obtained by assuming that the shift factors for pressure and concentration are separable, and the Fujita−Kishimoto model was found to describe the effect of concentration alone on the concentration shift factor. The effects of carbon dioxide and nitrogen were found to be the same if the concentration is expressed in moles.

## 1. Introduction

Supercritical fluids (SCFs) have been evaluated as solvents and extraction agents in the food, pharmaceutical, and chemical industries[1−10] and are also used in the plastics industry.[11−15] In particular, supercritical carbon dioxide (SC-$CO_2$) has been used as a physical blowing agent in plastic foam production and as a plasticizer to reduce melt viscosity for melt processing. It is known that a dissolved SCF reduces melt viscosity even at elevated pressures, and this makes it possible to process some polymers that are normally hard to process due to a high melt viscosity. For example, an SCF can dissolve fluoropolymers that are insoluble in most solvents[16] except SCFs and chlorofluorocarbons (CFCs). Releasing CFCs into the atmosphere has been found to enhance global warming[17] and damage the ozone layer,[18] and the Montreal Protocol (1987) and Copenhagen Amendment (1992)[19] mandated phaseout of the use of CFCs by 1996. Hydrocarbons, which are currently used as physical blowing agents, are highly flammable, and their use requires special safety precautions. Moreover, the global warming potential of hydrocarbons[17,20] is higher than that of $CO_2$. Nitrogen ($N_2$) has a lower critical temperature and pressure (−146.9 °C and 3.4 MPa) than those of $CO_2$ (31.0 °C and 7.4 MPa) and has much less solubility in molten polymers than that of $CO_2$. Nitrogen is a good candidate for processing of fine-cellular foams, and $CO_2$ is good for producing low-density foams. Both are also easy to obtain and remove, cheap, and nontoxic and cause no ozone depletion. For the above reasons, SC-$CO_2$ and SC-$N_2$ are very attractive SCFs for the polymer industry.

Although elevated pressures are involved in several important polymer processing operations, such as high-speed extrusion and injection molding, few studies of the pressure dependence of rheological properties such as viscosity have been reported due to the difficulty of carrying out experiments at a uniform, high pressure. Data reported to date were obtained using capillary or slit rheometers,[21−30] and the temperature, pressure, and shear rate are not uniform in these instruments. Falling-cylinder[31,32] and Couette viscometers[33] have also been used to measure viscosity at high pressure, but only at very low shear rates.

A high-pressure sliding plate rheometer (HPSPR) was used in the present study. In this instrument, the temperature, pressure, dissolved gas concentration, and shear rate are all uniform. Also, the pressure and concentration of dissolved gas can be controlled independently of the shear rate. The shear stress is measured using a shear stress transducer, which senses the stress in the center of the sample so that edge effects are not a problem.

## 2. Method of Reduced Variables and Viscosity Models

The method of reduced variables[34] is an essential tool for describing the dependency of rheological properties on temperature, pressure, and concentration. A material whose temperature and shear rate dependency can be represented in terms of reduced variables is said to be thermorheologically simple or to exhibit time−temperature superposition. And a material whose pressure and shear rate dependency can be represented in terms of reduced variables is said to be piezorheologically simple or to exhibit time−pressure superposition. To generate a master curve of shear stress or viscosity versus shear rate that brings together data obtained at several temperatures or pressures, horizontal and vertical shift factors were used.

* Corresponding author. E-mail: john.dealy@mcgill.ca.
† E-mail: heanpark@dreamwiz.com.

10.1021/ma060735+ CCC: $33.50 
Published on Web 07/14/2006

On the basis of thermodynamic arguments,[35] stresses should scale with the product of polymer density and temperature.[34] For a pure polymer, therefore, the vertical temperature shift factor $b_T$ for stress should be:

$$b_T(T) \equiv \frac{\rho_{pol}(T)T}{\rho_{pol}(T_0)T_0} \tag{1}$$

where $T$ is temperature, $\rho_{pol}$ is the density of polymer, and the subscript zero indicates the reference conditions. For a solution,[34] the density is replaced by the polymer concentration $C_{pol}$, expressed in the same units as density (g/cm$^3$), and the factor becomes

$$b_{T,C}(T, C) \equiv \frac{C_{pol}(T, C)T}{\rho_{pol}(T_0, C_0)T_0} \tag{2}$$

where $C$ is the concentration of the dissolved material, which is often used as the independent variable for shift factors because it can be controlled directly, and $C_{pol}$ is defined by eq 3:

$$C_{pol}(T, C) \equiv \frac{W_{pol}}{V_m(T, C)} \tag{3}$$

where $W_{pol}$ is the weight of pure polymer in the solution, and $V_m$ is the volume of the mixture.

If pressure is also varied, the effect of pressure on density must be taken into account, and the vertical shift factor is given by:

$$b_{T,P}(T, P) \equiv \frac{\rho_{pol}(T, P)T}{\rho_{pol}(T_0, P_0)T_0} \tag{4}$$

where $P$ is pressure. If only the pressure is varied, with $T = T_0$, we obtain a vertical shift factor for pressure alone:

$$b_P(P) \equiv \frac{\rho_{pol}(P)}{\rho_{pol}(P_0)} \tag{5}$$

Finally, the vertical $T$, $P$, and $C$ shift factor is given by:

$$b_{T,P,C}(T, P, C) \equiv \frac{C_{pol}(T, P, C)T}{\rho_{pol}(T_0, P_0, C_0)T_0} \tag{6}$$

The vertical shift factors can be obtained by pressure−volume−temperature ($PVT$) measurement.

The use of a horizontal temperature shift factor $a_T(T)$ for time, frequency, or shear rate is based on the assumption that all the times of the relaxation spectrum are equally affected by temperature. While this not valid over very broad ranges of the time variable,[36] it works quite well over a limited range such as that employed in the present study, in which the shear rate varied from $10^{-4}$ to 60 s$^{-1}$. A temperature-independent master curve is thus obtained by plotting $\sigma/b_T$ versus $\dot{\gamma}a_T(T)$ or $\eta/a_Tb_T$ versus $\dot{\gamma}a_T(T)$, where $\sigma$ is the shear stress. If the zero-shear viscosity $\eta_0(T)$ is known, the horizontal shift factor can be determined by:

$$a_T(T) = \frac{\eta_0(T)}{\eta_0(T_0)}\frac{1}{b_T(T)} \tag{7}$$

If the zero-shear viscosity is not known, the horizontal shift factor can be determined by using a least-squares method to identify the $a_T(T)$ function that best superposes data obtained over a range of shear rates. This involves plots of $\sigma/b_T$ versus shear rate, where the shift is carried out only along the shear rate axis rather than plots of viscosity versus shear rate, which require shifts along both axes. A temperature-independent master curve can then be constructed by plotting:

$$\frac{\eta(T)}{a_T(T)b_T(T)} \text{ versus } \dot{\gamma}a_T(T) \tag{8}$$

This implies that the effect of temperature on the zero-shear viscosity can be described by:

$$\eta_0(T) = a_T(T)b_T(T)\eta_0(T_0) \tag{9}$$

However, the vertical shift factor is often omitted, as it is rarely far from one, especially for crystallizable polymers, due to the limited test range that are experimentally accessible. When this is the case, the horizontal temperature shift factor is reduced to:

$$a'_T(T) = \frac{\eta_0(T)}{\eta_0(T_0)} \tag{10}$$

where the prime is added to distinguish this factor from the $a_T$ where $b_T \neq 1$ because the horizontal temperature shift factor ignoring $b_T$ will be different from that when $b_T$ is used. A temperature-independent viscosity plot for this case is then constructed by plotting:

$$\frac{\eta(T)}{a'_T(T)} \text{ versus } \dot{\gamma}a'_T(T) \tag{11}$$

Because $a'_T(T)$ is proportional to $\eta_0(T)$ for a given polymer, i.e., the same $\eta_0(T_0)$, the above equations can be combined to show that a temperature-independent plot can be obtained by plotting:

$$\frac{\eta(T)}{\eta_0(T)} \text{ versus } \dot{\gamma}\eta_0(T) \tag{12}$$

if $\eta_0(T)$ is known.

If pressure also affects all the time constants similarly, a horizontal pressure shift factor $a_P(P)$ is used to bring together data obtained at one temperature but several pressures. Thus, one would obtain a pressure-independent master curve by plotting $\sigma/b_P$ versus $\dot{\gamma}a_P(P)$ or $\eta/a_Pb_P$ $\dot{\gamma}a_P(P)$. If the zero-shear viscosity $\eta_0(P)$ is known, the horizontal shift factor can be determined by:

$$a_P(P) = \frac{\eta_0(P)}{\eta_0(P_0)}\frac{1}{b_P(P)} \tag{13}$$

If the zero-shear viscosity is not known, the horizontal shift factor can be determined by using a least-squares method to identify the $a_P(P)$ function that best superposes data obtained over a range of shear rates. This involves plots of $\sigma/b_P$ versus shear rate, where the shift is carried out only along the shear rate axis rather than plots of viscosity versus shear rate, which require shifts along both axes. A pressure-independent master curve can then be constructed by plotting:

$$\frac{\eta(P)}{a_P(P)b_P(P)} \text{ versus } \dot{\gamma}a_P(P) \tag{14}$$

The effect of pressure on the zero-shear viscosity is given by:

$$\eta_0(P) = a_P(P)b_P(P)\eta_0(P_0) \tag{15}$$

The vertical pressure shift factor is often omitted, and the horizontal pressure shift factor is then reduced to:

$$a'_P(P) = \frac{\eta_0(P)}{\eta_0(P_0)} \tag{16}$$

where the prime is added to distinguish this factor from the $a_P$ where $b_P \neq 1$. A pressure-independent viscosity plot for this case is thus obtained by plotting:

$$\frac{\eta(P)}{a'_P(P)} \text{versus } \dot{\gamma}a'_P(P) \tag{17}$$

If $\eta_0(P)$ is known, a pressure-independent plot can be obtained by plotting:

$$\frac{\eta(P)}{\eta_0(P)} \text{ versus } \dot{\gamma}\eta_0(P) \tag{18}$$

In the case of a polymer solution at $P$ and $C$, the vertical shift factor $b_{P,C}$ is likely to be necessary because a solvent can have a much larger effect on polymer density than temperature or pressure, The procedure to obtain $a_{P,C}$ or $\eta_0(P, C)$ is the same as the case of a polymer melt at $T$ or $P$. Thus, to obtain a master curve of data taken at various values of $P$ and $C$, one should plot:

$$\frac{\eta(P, C)}{a_{P,C}(P, C)b_{P,C}(P, C)} \text{ versus } \dot{\gamma}a_{P,C}(P, C) \tag{19}$$

Or if the zero-shear viscosity is known, one can also obtain a master curve by plotting:

$$\frac{\eta(P, C)}{\eta_0(P, C)} \text{ versus } \dot{\gamma}\eta_0(P, C)/b_{P,C}(P, C) \tag{20}$$

If the solubility of the solvent is very low or the solvent swells the polymer very little, the vertical shift factor can be assumed to be one, and the following plot can be made:

$$\frac{\eta(P, C)}{a'_{P,C}(P, C)} \text{ versus } \dot{\gamma}a'_{P,C}(P, C) \tag{21}$$

where $a'_{P,C}(P, C)$ is the combined pressure and concentration shift factor assuming $b_{P,C}$ to be one.

To study the dependency or sensitivity of rheological properties on $T$, $P$, or $C$, it is necessary to inspect a plot of the slope of a shift factor versus $T$, $P$, or $C$ instead of the absolute value of the shift factor, which is arbitrary because it changes depending on the reference conditions. In this study, all experiments were performed at one temperature, and further analysis will be carried out using only pressure and concentration as state variables. To describe the dependency of viscosity on $P$ and $C$, two models were used. Well above the melting temperature, an exponential equation that is equivalent to Barus' relationship[37] can often be used to describe the pressure shift factor:

$$\ln\left[\frac{\eta_0(P)}{\eta_0(P_0)}\right] = \ln[a_P(P)b_P(P)] = \beta(P - P_0) \tag{22}$$

where $\beta$ is a constant often called the pressure coefficient of viscosity and is defined as:

$$\beta \equiv \frac{1}{\eta_0}\left(\frac{\partial\eta_0}{\partial P}\right)_T \tag{23}$$

The pressure coefficient is a function of molecular structure but not of $\dot{\gamma}$ or $P$, if the material is piezorheologically simple. Fujita and Kishimoto[38] derived an equation analogous to the WLF equation[39] for the effect of dissolved gas on the viscosity of a polymer based on the free volume concept:

$$\ln[a_C(C)] = \frac{(-1/f)C}{f/\theta + C} \tag{24}$$

where $a_C$ is the horizontal concentration shift factor, $f$ is the fractional free volume, i.e., the ratio of free volume to total volume, and $\theta$ is the contribution of the dissolved gas to the increase of free volume.

### 3. Polymer Studied

A high-density polyethylene was chosen due to its commercial importance. Our sample was provided by Japan Polyolefins (formerly Nippon Petrochemicals) and is a general-purpose film resin. The same material has been previously studied by Sato et al.,[40] who reported the solubility and diffusion coefficient for $CO_2$ and $N_2$ in this polymer. The melting/crystallization temperatures were determined at 1 atm by the use of a differential scanning calorimeter (DSC) with a heating/cooling rate of 10 °C/min. Two melting temperatures were identified, one ($T_{m,h}$) from the peak in the endothermic curve and the other ($T_{m,e}$) from the end of the peak. Crystallization temperatures were defined in the same manner. The results are summarized in Table 1.

### 4. Pressure−Volume−Temperature Behavior of Pure Polymer

Because the melting point $T_m$ increases with pressure, to prevent pressure-induced crystallization, the high-pressure measurements must be carried out at temperatures well above the elevated $T_m$. The pressure dependencies of $T_m$ were obtained by determining the *PVT* behavior of the polymer. This information is also needed to determine the solubility of the gas in the polymer and the vertical shift factor for viscosity.

We used the empirical Tait equation to describe our *PVT* data for pure polymer. Tait[41] fitted his data for the average isothermal compressibility for fresh water and seawater using the following equation:

$$-\frac{1}{v(P_0, T)}\frac{v(P, T) - v(P_0, T)}{P} = \frac{C(T)}{B(T) + P} \tag{25}$$

where $v(P_0, T)$, $B(T)$, and $C(T)$ are functions of temperature only. Wohl[42] modified and integrated eq 25 to give eq 26, if we take $P_0$ to be zero.

$$v(P, T) = v(0, T)\left\{1 - C(T)\ln\left[1 + \frac{P}{B(T)}\right]\right\} \tag{26}$$

Cutler et al.[43] found that $C(T)$ has a universal value of 0.0894 for high-molecular-weight hydrocarbons and is independent of temperature. Equation 26 can thus be reduced to eq 27:

$$v(P, T) = v(0, T)\left\{1 - 0.0894\ln\left[1 + \frac{P}{B(T)}\right]\right\} \tag{27}$$

where the zero-pressure isotherm that we used is given by:

$$v(0, T) = v_0 + v_1T \tag{28}$$

**Table 1. Physical Properties of HDPE.**

| density (24.5 ° C) | $M_w$[40] kg/mol | $M_w/M_n$[40] kg/mol | $T_{m,h}$ °C | $T_{m,e}$ °C | $T_{c,h}$ °C | $T_{c,e}$ °C |
|---|---|---|---|---|---|---|
| 0.945 | 111 | 13.6 | 130.5 | 134.4 | 115.7 | 113.1 |

and $B(T)$ is given by

$$B(T) = B_0\, e^{-B_1 T} \tag{29}$$

where $v_0$, $v_1$, $B_0$, and $B_1$ are constants. Wohl's modification, eq 27, has been called the Tait model and widely used to describe the *PVT* behavior of polymers.

To predict the effect of dissolved $CO_2$ on the melt volume to obtain the solubility of $CO_2$, a theoretical model was required because mixing rules for the parameters are available only for such models. For this study, the Sanchez−Lacombe (SL) model[44] was chosen because it has a simple structure and has been used previously to describe the solubility of $CO_2$.[40,46,47] The SL model can be expressed as follows in terms of reduced variables:

$$\tilde{P} = -\tilde{\rho}^2 - \tilde{T}\left[\ln(1-\tilde{\rho}) + \left(1-\frac{1}{r}\right)\tilde{\rho}\right] \tag{30}$$

where $\tilde{T} \equiv T/T^*$, $\tilde{P} \equiv P/P^*$, and $\tilde{\rho} \equiv \rho/\rho^*$. The characteristic values are $T^* \equiv \epsilon^*/R$, where $R$ is the gas constant, $P^* \equiv \epsilon^*/v^*$, and $\rho^* \equiv M/(rv^*)$. The close-packed mer volume is $v^* \equiv RT^*/P^*$, and $\epsilon^*$ is the interaction energy. The number of mers per molecule, i.e., the number of lattice sites occupied by a molecule is $r \equiv M/(v^*\rho^*) = MP^*/(RT^*\rho^*)$, where $M$ is the molecular weight. Either ($\epsilon^*$, $R$, $v^*$) or ($T^*$, $P^*$, $\rho^*$) is determined by curve fitting.

A Gnomix *PVT* apparatus[48] was used isothermally to determine the *PVT* behavior of HDPE. The effects of temperature and pressure on the specific volume of HDPE are shown in Figure 1, where the melt, transition, and solid zones can be readily identified. The curve at 135 °C shows a large volume decrease starting at 40 MPa, and the 140 °C isotherm shows a large decrease starting at 60 MPa. At 145 °C, however, pressurizing up to 80 MPa cannot solidify the sample. The temperature used in our work was 180 °C, which is certain to be in the melt zone at all pressures of interest. Figure 2 shows the effect of pressure on $b_P(P) \equiv \rho_{pol}(P)/\rho_{pol}(P_0)$ at 180 °C. There is a 6% variation from one atmosphere up to 70 MPa.

Capt and Kamal[49] found that it is better to determine the four parameters of the Tait model in one nonlinear regression rather than determine them by separate regressions. Our results are

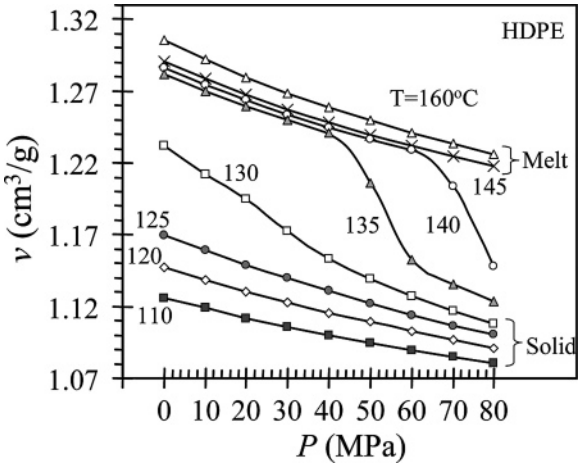


**Figure 1.** The effect of temperature and pressure on the specific volume of HDPE. (Lines show trends only, not model predictions.)

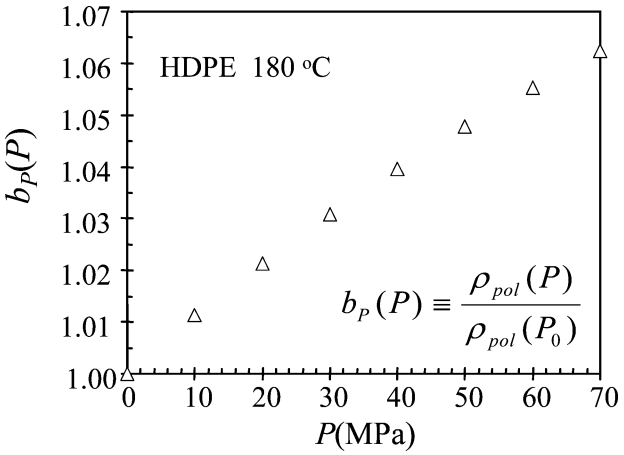


**Figure 2.** Effect of pressure on $b_P(P)$ of HDPE at 180 °C.

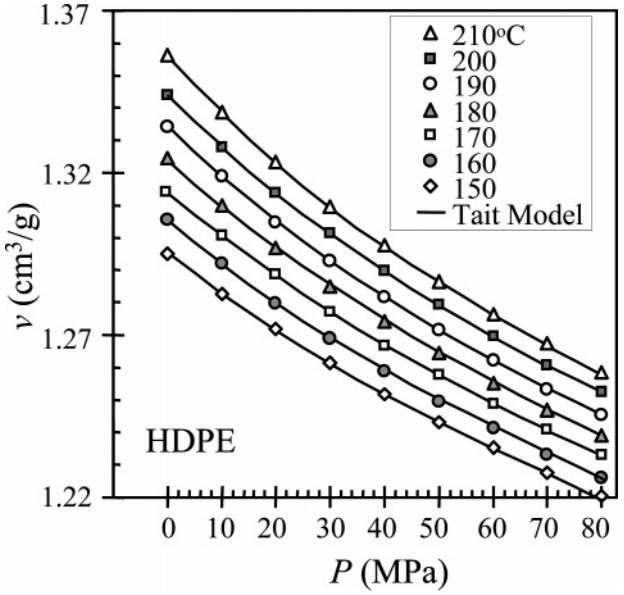


**Figure 3.** Comparison of *PVT* data with Tait model predictions.

**Table 2. Comparison of Our Tait Model Parameters for HDPE with Those of Rodgers**

| parameter units | $v_0$ cm³/g | $v_1$ cm³/gK or cm³/g °C | $B_0$ MPa | $B_1$1/K or 1/ °C |
|---|---|---|---|---|
| this work ($T$ in K) | 0.876 | $9.84 \times 10^{-4}$ | 677.0 | $4.83 \times 10^{-3}$ |
| this work ($T$ in °C) | 1.145 | $9.85 \times 10^{-4}$ | 181.7 | $4.84 \times 10^{-3}$ |
| Rodgers[50] ($T$ in °C) | 1.160 | $8.04 \times 10^{-4}$ | 179.9 | $4.74 \times 10^{-3}$ |

compared with data of Rodgers[50] and given in Table 2. We prefer temperature in K for calculations, but the parameters obtained using $T$ in °C are also given because Rodgers reported the Tait parameters when $T$ was expressed in °C. The difference between two sets of parameters is small considering that different polymers were studied. Our data, together with the curves calculated using the Tait model, are shown in Figure 3.

Unlike the Tait equation, the Sanchez−Lacombe (SL) equation does not give the volume explicitly. To calculate the specific volume, two steps are required using eq 30. First, model fitting is carried out by determining the parameters that minimize the error sum $ES$:

$$ES \equiv \sum_{i=1}^{Q}\left\{\tilde{P}_i + \tilde{\rho}_i^{\,2} + \tilde{T}_i\left[\ln(1-\tilde{\rho}_i) + \left(1-\frac{1}{r}\right)\tilde{\rho}_i\right]\right\}^2 \tag{31}$$

where $i$ is the pressure and temperature index, and $Q$ is the

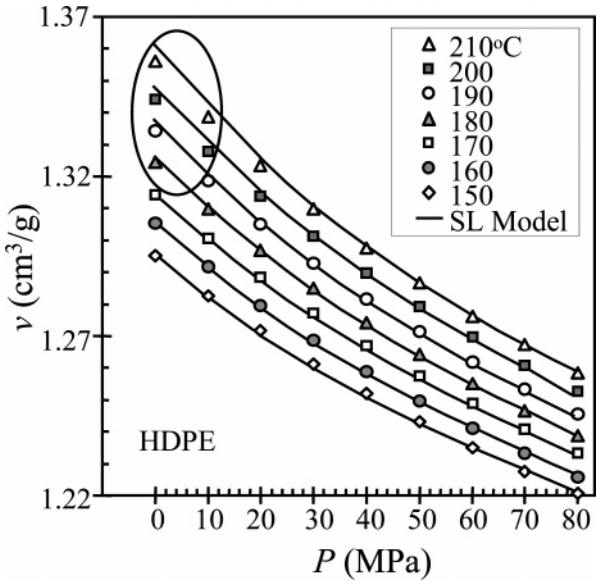


**Figure 4.** Comparison of *PVT* data with SL model prediction.

**Table 3. Comparison of Our SL Parameters for HDPE with Those of Rodgers and Those for Carbon Dioxide**

| parameter | $P^*$ MPa | $T^*$ K | $\rho^*$ g/cm$^3$ |
|---|---|---|---|
| HDPE: this work | 388.8 | 640 | 0.890 |
| HDPE: Rodgers[50] | 366.2 | 615 | 0.914 |
| $CO_2$: this work | 727.4 | 319 | 1.725 |

number of data. Second, using the data sets ($T_i$, $P_i$) and the parameters determined in the first step, reduced densities $\tilde{\rho}_{c,i}$ are calculated in the following equation using Newton's method:

$$\tilde{P}_i + \tilde{\rho}_{c,i}^{\,2} + \tilde{T}_i\left[\ln(1-\tilde{\rho}_{c,i}) + \left(1-\frac{1}{r}\right)\tilde{\rho}_{c,i}\right] = 0 \quad (32)$$

Finally, the calculated specific volume is obtained from:

$$v_{c,i} = \frac{1}{\tilde{\rho}_{c,i}\rho^*} \quad (33)$$

The parameters determined in the present study are compared with those of Rodgers[50] in Table 3, and the difference is minor. The resulting parameters will be used to obtain the specific volume of HDPE/$CO_2$ mixture in the section on solubility. As shown in Figure 4, the SL model provides a less-accurate description of pure polymer than the Tait model and significantly overestimates the volume at high temperature and low pressure (ellipse in Figure 4).

### 5. Gas Solubility and Swollen Polymer Volume

Because the rheometer we used operates only at the saturation concentration, the solubility ($S$) must be known. A magnetic suspension balance (MSB) manufactured by Rubotherm was used to determine the amount of dissolved $CO_2$. The buoyancy effect in a measurement cell changes the net weight of HDPE/$CO_2$ mixture. To account for buoyancy, the *PVT* data described in the section on *PVT*, together with the $CO_2$ density determined using the MSB, were combined with data obtained using the MSB ignoring buoyancy. To determine the solubility, the swollen volume of polymer is also required, and the Sanchez−Lacombe (SL) model was used to analyze the data because that could not be measured directly. The swollen volume of polymer obtained here was also used in the form of a vertical shift factor. Literature solubility data[40] were used for $N_2$. The polymer is assumed to be immobile due to its high molecular weight, so gas dissolves in the polymer, and the gas phase contains no polymer. At equilibrium, the chemical potential of gas in the gas phase is equal to that in the polymer/gas mixture phase, and the concentration of gas in the mixture is the solubility.

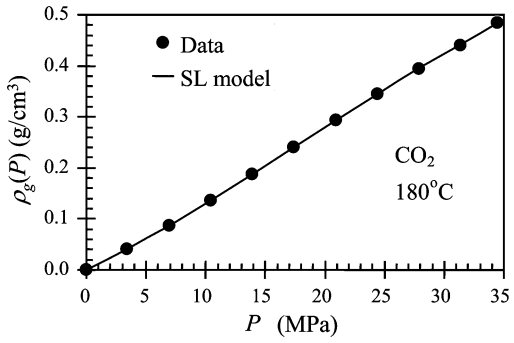


**Figure 5.** Effect of pressure on $CO_2$ density and comparison with SL model prediction.

The Sanchez−Lacombe model[44] was used to calculate the volume of polymer swollen with $CO_2$, since it has been shown to be useful for polymers containing $CO_2$.[40,51] The SL equation for a mixture can be written as:

$$\tilde{P}_m = -\tilde{\rho}_m^{\,2} - \tilde{T}_m\left[\ln(1-\tilde{\rho}_m) + \left(1-\frac{1}{r_m}\right)\tilde{\rho}_m\right] \quad (34)$$

where $\tilde{T}_m \equiv T/T_m^*$, $\tilde{P}_m \equiv P/P_m^*$, and $\tilde{\rho}_m \equiv \rho_m/\rho_m^*$. Each parameter for the mixture is related to those of the pure components by a mixing rule[45,52] (Appendix). However, the mixing rule contains at least one interaction parameter, which cannot be predicted, and the equation of state is thus not predictive. We derived a special form of the SL model for the case of a two-component and two-phase system in which only one component is soluble in the other. The derivation is given in the Appendix, and the resulting equation is shown as eq 35

$$r_1^{\,0}RT\left[-\frac{\tilde{\rho}_1}{\tilde{T}_1} + \frac{\tilde{P}_1}{\tilde{\rho}_1\tilde{T}_1} + \left(\frac{1}{\tilde{\rho}_1}-1\right)\ln(1-\tilde{\rho}_1) + \frac{1}{r_1^{\,0}}\ln\tilde{\rho}_1\right]$$
$$= RT\left[\ln\phi_1 + \left(1-\frac{r_1}{r_2}\right)\phi_2 + r_1^{\,0}\tilde{\rho}_m\frac{P_1^*+P_2^*-2P_{12}^*}{P_1^*\tilde{T}_1}\phi_2^{\,2}\right] +$$
$$r_1^{\,0}RT\left[-\frac{\tilde{\rho}_m}{\tilde{T}_1} + \frac{\tilde{P}_1}{\tilde{\rho}_m\tilde{T}_1} + \left(\frac{1}{\tilde{\rho}_m}-1\right)\ln(1-\tilde{\rho}_m) + \frac{1}{r_1^{\,0}}\ln\tilde{\rho}_m\right] \quad (35)$$

A number of methods have been used to measure the solubility of a gas in a polymer.[11] Funami et al.[47] found that the agreement between the direct determination and indirect prediction using the SL model was excellent. For the present study, we chose an indirect method in which data are used together with an equation of state to determine both the solubility and the swollen volume.[40,46,53,54] A magnetic suspension balance (MSB) manufactured by Rubotherm was used to measure the density of $CO_2$ and the weight change of HDPE due to dissolved $CO_2$. The method of data analysis can be found elsewhere.[46,53,55] Figure 5 shows the effect of pressure on the density of $CO_2$ at 180 °C and pressures from 0.1 to 34.5 MPa. These data were used to obtain the parameters of the SL model for $CO_2$ and to determine the buoyancy effect. The parameters were determined by the least-squares method using as initial guesses values reported by Areerat et al.[56] for an MSB system. The parameters of the SL model for $CO_2$ are given in Table 3, and those for HDPE were determined by *PVT* measurements. These were used

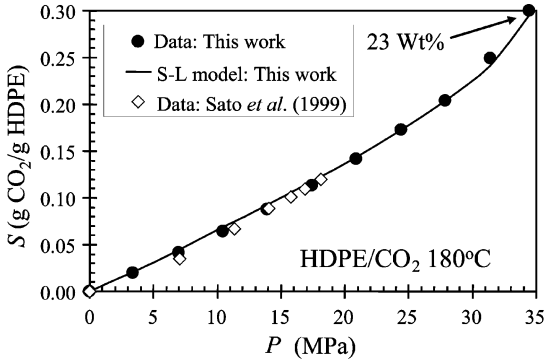


**Figure 6.** Effect of pressure on the $CO_2$ solubility in HDPE.

**Table 4. Solubility of Carbon Dioxide in HDPE**

| | solubility (180 °C) | |
|---|---|---|
| pressure MPa | g $CO_2$/kg HDPE | mol $CO_2$/kg HDPE |
| 0.0 | 0 | 0.0 |
| 3.4 | 20 | 0.4 |
| 7.0 | 42 | 0.9 |
| 10.5 | 64 | 1.5 |
| 14.0 | 88 | 2.0 |
| 17.4 | 113 | 2.6 |
| 20.9 | 141 | 3.2 |
| 24.4 | 172 | 3.9 |
| 27.9 | 204 | 4.6 |
| 31.3 | 249 | 5.7 |
| 34.5 | 300 | 6.8 |

**Table 5. Solubility of Nitrogen in HDPE**

| | solubility (180 °C)[40] | |
|---|---|---|
| pressure MPa | g $N_2$/kg HDPE | mol $N_2$/kg HDPE |
| 0.0 | 0.0 | 0.0 |
| 3.7 | 3.7 | 0.13 |
| 6.3 | 6.6 | 0.23 |
| 8.2 | 8.5 | 0.30 |
| 9.4 | 9.7 | 0.34 |
| 11.8 | 12.6 | 0.45 |

to determine the parameters of the SL model for the mixture by using the mixing rule.

Figure 6 shows the solubility increase with pressure. At 34.5 MPa, the solubility reaches 0.3 g $CO_2$/g HDPE and 23 wt % (100 g $CO_2$/g mixture). The solubilities obtained in this work were compared with those for the same HDPE that were reported by Sato et al.,[40] who used the pressure decay method. To estimate the swollen volume, they used literature values for the $CO_2$ parameters of the SL model rather than determining them experimentally. Figure 6 shows that there is a little difference between their data and those of this study. Table 4 shows the solubility of $CO_2$ in HDPE measured in this work, and Table 5 shows values for $N_2$ that were reported by Sato et al.[40]

Figure 7 shows the mixture volume as a function of pressure. A 32% increase of the mixture volume was observed at 34.5 MPa. The linear swell factor $k$ can be obtained from the mixture volume as:

$$k^2(P, C) \equiv V_m(P, C)/V_{pol}(P_0) \tag{36}$$

where $V_m$ and $V_{pol}$ are the volumes of mixture and pure polymer, respectively, and is used in the section on diffusion to study the effect of the moving boundary. The power of 2 instead of 3 is used for the swell factor because a sample swells in only two directions in the HPSPR. For example, $k^2$ (18 MPa) = 1.14, and $k^2$ (34.5 MPa) = 1.32.

Figure 8 shows the effect of $CO_2$ pressure on the vertical shift factor defined as eq 37:

$$b_{P,C}(P, C) \equiv \frac{C_{pol}(P, C)}{\rho_{pol}(P_0)} = \frac{W_{pol}/V_m(P, C)}{W_{pol}/V_{pol}(P_0)} = \frac{V_{pol}(P_0)}{V_m(P, C)} = \frac{1}{k^2} \tag{37}$$

where $W_{pol}$ is the weight of the pure polymer. There is a 24% decrease of $b_{P,C}(P, C)$ at 34.5 MPa, and this is large enough to affect the rheological properties. This will be used for the study for the effect of $CO_2$ on viscosity.

### 6. Diffusion of $CO_2$ in Polymer

To obtain reliable results, experiments must be carried out while the sample is saturated with an SCF, which is used to pressurize the melt, at each pressure, as the high-pressure sliding plate rheometer does not permit independent control of pressure and concentration. The saturation process takes a long time, as diffusion occurs only from the thin edges of the sample, which is sandwiched by moving and fixed plates of the HPSPR. A polymer with too long a saturation time cannot be used because of thermal degradation. It was thus of interest to estimate the time required to achieve uniform saturation. We assumed two-dimensional Fickian diffusion[57,58] with a constant diffusion coefficient $D$ to calculate both the gas concentration at the center of the sample as a function of time $C_0(t)$ and the total mass of gas absorbed $M(t)$.[59] We used the value of $D$ for $CO_2$ in HDPE that was reported by Sato,[40] which was $9 \times 10^{-5}$ cm$^2$/s at 180 °C and only a weak function of pressure.

Figure 9 shows plots of dimensionless center concentration $C_0(t)/S$, and total mass absorbed $M(t)/M(\infty)$ versus dimensionless diffusion time, where $M(\infty)$ is the absorbed quantity after infinite time. The key feature of this plot for our purposes is the time required to reach 99% saturation. The sample dimensions are 1.6 cm × 8.0 cm, so $a$ (the length-to-width ratio) is 5, and $L$ (half the sample width) is 0.8 cm. The values of $Dt/L^2$ are 1.64 for $M(t)/M(\infty) = 0.99$ and 1.96 for $C_0(t)/S = 0.99$. The corresponding times for 99% saturation in terms of $C_0(t)/S$ and $M(t)/M(\infty)$ are then 194 and 230 min, respectively. Our HDPE had sufficient thermal stability to make viscosity measurements feasible, but the situation varies greatly depending on the diffusivity of $CO_2$ in the polymer. For example, in the case of polystyrene, about 2 days are required to achieve 99% saturation at the center of the sample.

The points shown in Figure 10 are based on viscosity measurements and the curves are model predictions for $C_0(t)/S$ and $M(t)/M(\infty)$. The point at time zero is the viscosity without $CO_2$ at 18 MPa and is assumed to be the viscosity at time zero after applying 18 MPa of $CO_2$. We made viscosity measurements every 20 min during the diffusion process, and the points shown are the relative viscosity defined as

$$\eta_R(t) \equiv \frac{\eta(t) - \eta(0)}{\eta(\infty) - \eta(0)} \tag{38}$$

where $\eta(\infty)$ is the viscosity at saturation. The shear stress transducer of the HPSPR measures the shear force on a small area in the center of the sample, and the viscosity data are thus expected to be between $C_0(t)/S$ and $M(t)/M(\infty)$. However, Figure 10 shows that the viscosity matches $C_0(t)/S$ quite well. This results from our ignoring polymer swell and results in underestimating the diffusion time. If swell is considered, making this a moving boundary problem, the resulting predictions would be between those for unswollen and fully swollen polymer. The predictions in Figure 10 would need to be shifted to the right by less than 14% (for case of full swelling $k^2$ (18 MPa) = 1.14, Figure 7) to account for the moving boundary, and the viscosity

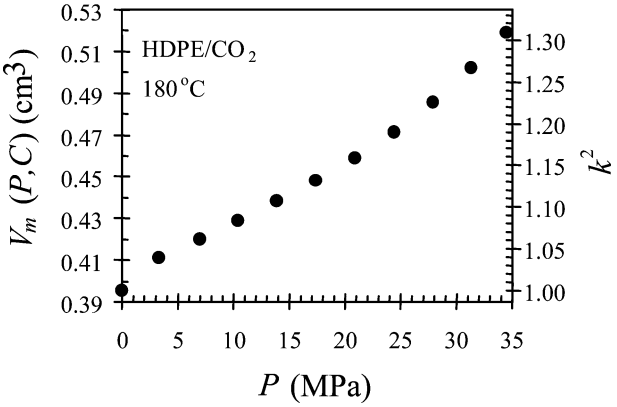


**Figure 7.** Effect of pressure on the volume of HDPE saturated with $CO_2$ and the linear swell factor. The weight of the pure polymer is 0.3 g.

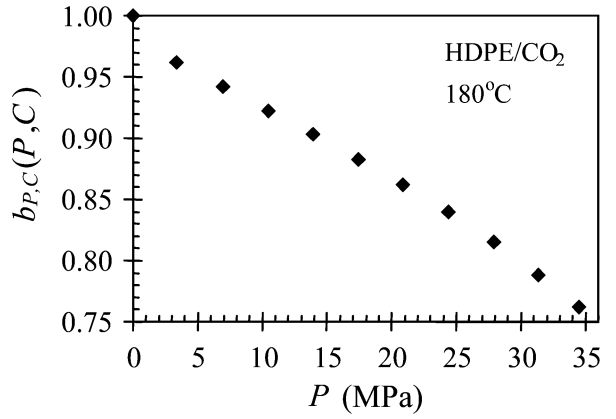


**Figure 8.** Effect of pressure on the concentration vertical shift factor.

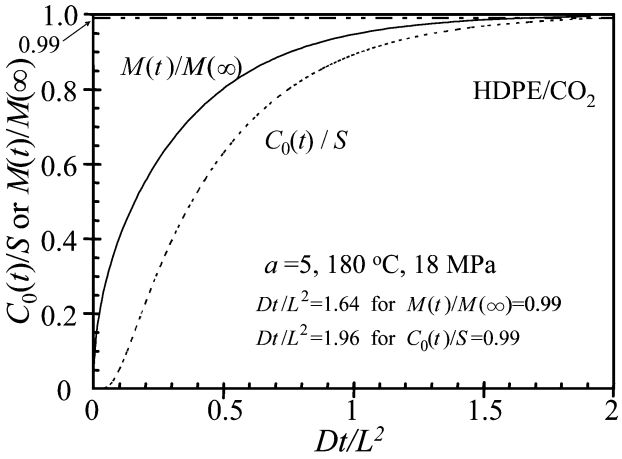


**Figure 9.** Dimensionless center concentration and mass absorbed vs dimensionless time.

data would then fall between $C_0(t)/S$ and $M(t)/M(\infty)$. We note that the viscosity data provide an excellent measure of the relative saturation at the center of the sample. This implies that viscosity measurements of this type could be used to determine the diffusion coefficient with reasonable accuracy. By contrast, the direct measurement of $D$ is difficult and subject to considerable uncertainty.

We found that subjecting the sample to continuous, oscillatory shear at a frequency of 0.01 Hz and a strain amplitude of 0.1 substantially accelerated the diffusion process. This is shown in Figure 11, which shows the viscosity in the center of the sample as a function of time, both with and without oscillatory shear. We see that the time for the viscosity to reach 99% saturation is reduced from 230 to about 120 min. The use of a higher frequency of 0.06 Hz did not further enhance the diffusion process and appeared to cause a shear instability that resulted in a marked fall off in viscosity after saturation had been achieved.

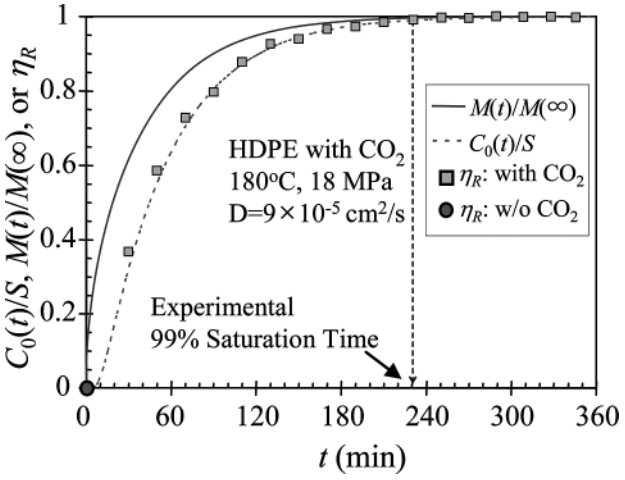


**Figure 10.** Comparison between experimental data showing the level of saturation and model prediction using a literature *D*: HDPE, 180 °C.

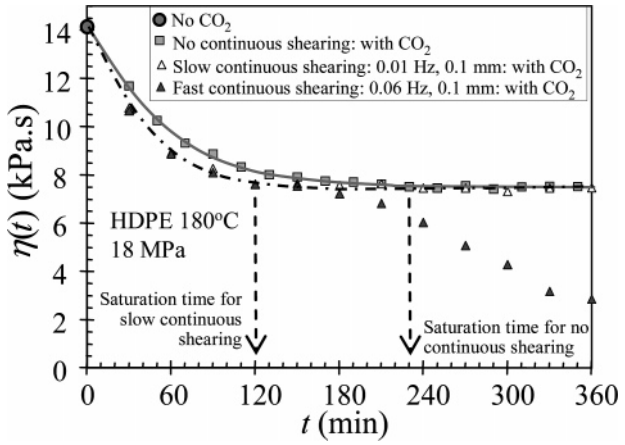


**Figure 11.** Effect of oscillatory shearing on the viscosity decrease during absorption of $CO_2$. The viscosity was measured at a shear rate of 0.63 $s^{-1}$. (Lines show trends only, not model predictions.)

## 7. Rheometers Used

**7.1. Rotational Rheometers.** An ARES rheometer (Rheometric Scientific) equipped with parallel disk fixtures (25 mm diameter and 1 mm gap) was used to determine the storage ($G'$) and loss ($G''$) moduli and the absolute value of complex viscosity ($|\eta^*|$) of pure polymer at 180 °C. Care was taken to ensure that all data were obtained at strains within the linear range and that thermo-oxidative degradation had no significant effect on the results. The results are shown in Figure 12. It was not possible to reach the classical low-frequency limiting behavior ($|\eta^*|$] constant; $G' \propto \omega^2$; $G'' \propto \omega$) at the lowest frequency used, which is not surprising given the polymer's broad molecular weight distribution.

To determine the viscosity of pure polymer at very low shear rates, a Rheometric Scientific SR5000 stress-controlled rheometer with cone-plate fixture was used. It was possible to reach shear rates of $8 \times 10^{-5}$ $s^{-1}$, but even at this very low rate, the viscosity was still varying slightly with shear rate.

**7.2. High-Pressure Sliding Plate Rheometer.** Giacomin et al.[60,61] developed a sliding-plate rheometer (SPR) incorporating

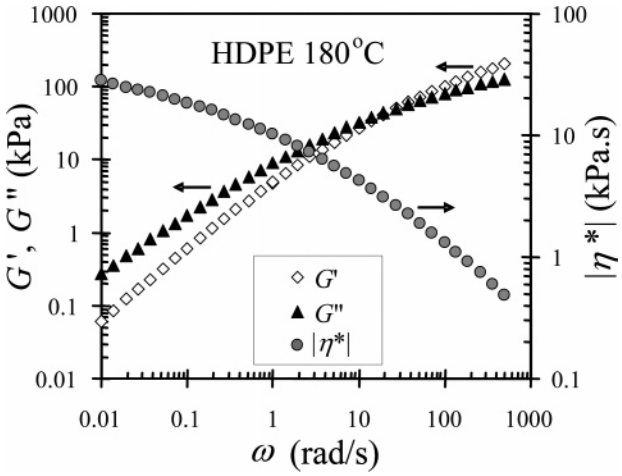


**Figure 12.** Dependency of moduli and complex viscosity on frequency for HDPE at 180 °C.

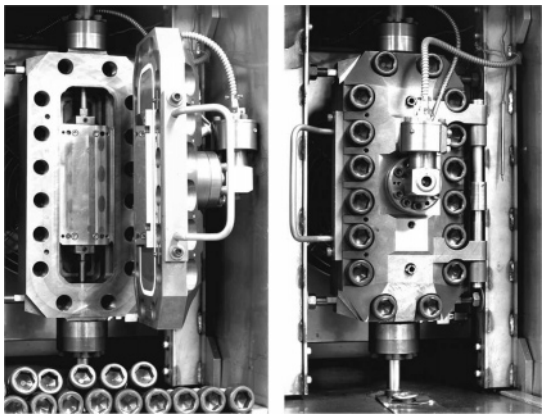

**Figure 13.** Photo of HPSPR in oven: (left) cover plate open; (right) cover plate closed.

a shear stress transducer, which has significant advantages over other types of rheometer for high shear rate studies, as the shear stress transducer measures stress at the center of the sample, and there are thus no end or edge effects. This instrument can generate controlled, homogeneous, linear shearing deformations at a uniform temperature in both strain- or stress-controlled modes. A high-pressure version of the sliding plate rheometer (HPSPR)[62,63] can generate shearing deformations at uniform pressure and temperature. It operates over a temperature range from 25 to 225 °C, under a vacuum or at pressures up to 70 MPa. It can generate shear rates from $10^{-3}$ to 500 $s^{-1}$ and can measure shear stresses up to 300 kPa. To study the effect of pure pressure, the rheometer is pressurized using Krytox general purpose oil 107 made by Dupont. This oil is thermally stable, nonflammable, nonvolatile, a good lubricant, and does not swell either polar or nonpolar materials. Figure 13 shows photos of the HPSPR in its oven.

The HPSPR was modified to allow for pressurization with an SCF for this study. The original high-pressure dynamic and static seals, fittings, and tubing system were redesigned to accommodate an SCF. Figure 14 is a schematic of the modified pressurizing system. Park[55] has described the modified system in detail. To study the combined effect of pressure and dissolved SCF, the rheometer was pressurized using an ISCO 100DM syringe pump. During an experiment, the line between the pump cylinder and the rheometer was left open to replace gas lost by absorption into the sample or due to small leaks. A vacuum pump was used to remove air from the rheometer and the sample prior to pressurization.

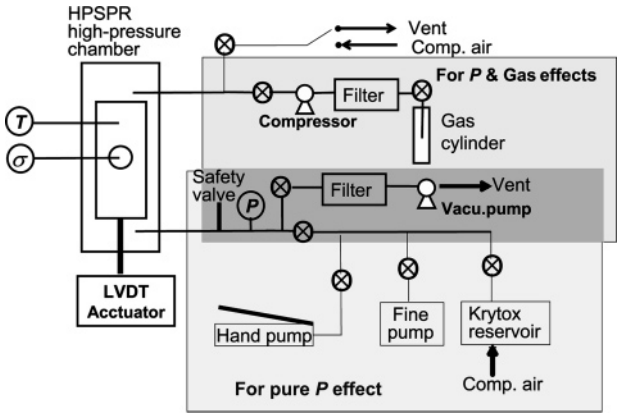


**Figure 14.** Schematic of pressurizing system.

To determine the effects of pressure and concentration, experiments were first performed using Krytox oil to determine the viscosity as a function of shear rate and pressure. The horizontal shift factors $a'_p(P)$ were obtained by shifting curves of shear stress versus shear rate at each pressure onto the curve for the reference state, which was 180 °C and 1 atm. Second, experiments were performed in an SCF environment. To confirm saturation of the sample as described in the section on diffusion, time sweep experiments were performed at each pressure prior to the shear-rate sweep experiments. After confirming the saturation time experimentally, a shear-rate sweep was performed at the same conditions as those used with Krytox, and the shift factors $a_{P,C}(P, C)$ for the combined effects of pressure and SCF were determined.

All tests were carried out with a gap of 1 mm and at a temperature of 180 °C. At the reference conditions of 1 atm and 180 °C, shear-rate sweep tests were repeated four times. There was a maximum 5% relative difference (*RD*) defined as follows.

$$RD \equiv \left(\frac{\text{highest} - \text{lowest}}{\text{lowest}}\right)_{\dot{\gamma},P,T} \times 100 \qquad (39)$$

At the other conditions, tests were repeated 1−3 times, and there was a maximum 6% relative difference.

## 8. Results and Discussion

**8.1. Viscosity of Polymer at One Atmosphere.** Viscosity information for pure polymer at 1 atm and 180 °C was available from three sources. The SR5000 provided data at shear rates between $8.0 \times 10^{-5}$ and $5.5 \times 10^{-4}$ $s^{-1}$, and the sliding plate rheometer gave results in the range from 0.1 to 40 $s^{-1}$. At intermediate shear rates, the viscosity was estimated using a corelation proposed by Cox and Merz.[64] On the basis of capillary viscometer data for two polystyrenes, they noted that a plot of complex viscosity versus frequency was very similar to that of apparent viscosity versus apparent shear rate. However, the so-called Cox−Merz rule as usually employed is the correlation shown by eq 40:

$$|\eta^*(\omega = \dot{\gamma})| = |\eta(\dot{\gamma})| \qquad (40)$$

The original observation of Cox and Merz, on the other hand, can be written as follows:

$$|\eta^*(\omega = \dot{\gamma}_A)| = \eta_A(\dot{\gamma}_A) \qquad (41)$$

The "apparent" viscosity and shear rate, $\eta_A$ and $\dot{\gamma}_A$, are calculated without taking into account the entrance pressure drop

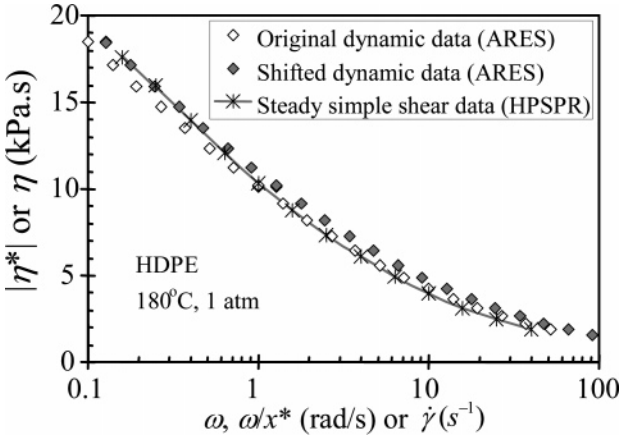


**Figure 15.** Comparison of viscosity with complex viscosity. $x^* = 0.79$. (Line shows a trend only, not a model prediction.)

and the non-Newtonian nature of the melt. It is probable that the entrance pressure drops for the polystyrene studied by Cox and Merz were small, but there would have been a significant difference between $\dot{\gamma}$ and $\dot{\gamma}_A$ due to the variation of viscosity with shear rate.

The rigorous method for determining the true shear rate from $\dot{\gamma}_A$ is the Rabinowitsch correction,[65] which is a tedious procedure requiring the differentiation of the $\eta_A(\dot{\gamma}_A)$ data. However, Schümmer et al.[66,67] showed that, for most non-Newtonian melts, the true viscosity curve to a good approximation can be obtained by a horizontal shift of $\eta_A(\dot{\gamma}_A)$ data as indicated by:

$$\eta_A(\dot{\gamma}_A) = \eta(\dot{\gamma}x^*) \tag{42}$$

where $x^*$ for capillary flow of a power-law fluid can be obtained by eq 43:[68]

$$x^* = \left(\frac{3n+1}{4n}\right)^{n/n-1} \tag{43}$$

where $n$ is a power-law constant. Combining eq 42 with the original Cox−Merz relation (eq 41), the latter now implies that viscosity data can be shifted horizontally to obtain the complex viscosity:

$$|\eta^*(\omega)| = \eta(\dot{\gamma}_A x^*) \tag{44}$$

Alternatively, complex viscosity can be shifted to give the viscosity:

$$\eta(\dot{\gamma}) = |\eta^*(\omega/x^*)| \tag{45}$$

Figure 15 compares viscosity versus shear-rate data with complex viscosity versus frequency data. The values of viscosity and complex viscosity do not agree perfectly, but the order of magnitude and shape of the two curves are similar. The viscosity shows slightly more shear thinning than the complex viscosity, and the two curves cross around 1 $s^{-1}$. In accordance with eq 45, the Schümmer shift factor[67] of 0.79 for $x^* = \pi/4$ was used, and the agreement between shifted complex viscosity curve and the viscosity is improved at low rates but worse at high rates. Indeed, the curvature of each data set is different, so the complex viscosity curve cannot be superposed onto the viscosity curve by shifting the entire curve on a semilogarithmic plot.

The Cross model[69] was found to describe the viscosity data. This is given by:

$$\eta(\dot{\gamma}) = \frac{\eta_0}{1 + |\lambda\dot{\gamma}|^m} \tag{46}$$

where $m$ is a fitting constant, $\eta_0$ is the zero-shear viscosity, and the characteristic time $\lambda$ is the inverse of the shear rate at which the viscosity is half its zero-shear value. As mentioned in the previous section, the zero-shear viscosity could not be determined directly from creep data, and an initial trial value was taken to be that at the lowest attainable shear stress from the creep tests. Viscosity values from both creep and steady shear tests, along with complex viscosity shifted by $x^*$ from Schümmer approximation, were fitted to eq 46, and the result is shown in Figure 16 for data at 1 atm. The complex viscosity data between 0.01 and 0.1 rad/s were fitted to the power-law model, and $n$ and $x^*$ were found to be 0.82 and 0.78, respectively. The zero-shear viscosity resulting from the curve fit is 37.3 kPa·s, $\lambda$ is 8.2 $s^{-1}$, and $m$ is 0.48 at 180 °C and 1 atm.

**8.2. Effect of Pressure on Viscosity.** Figure 17 shows viscosity versus shear-rate data at 180 °C and six pressures from 0.1 to 69 MPa. Data at 14 MPa are not shown to avoid confusion, but shifted data at this pressure will be presented. As is well-known, the viscosity increases with pressure. While $b_P(P)$ is usually assumed to be unity, this is not strictly true, and there is a 6% variation over 70 MPa for HDPE (Figure 2). However, the uncertainty in the accuracy of melt rheology data is of this order, and we took $b_P(P)$ to be unity. To determine the horizontal shift factor $a'_P(P)$ by the least-squares method, the stress versus shear rate curves for each $P$, as defined by the Cross model, were shifted along the horizontal axis onto that at $P_0$, as indicated by eq 47:

$$\sigma[\dot{\gamma}a'_P(P), P] = \sigma(\dot{\gamma}, P_0) \tag{47}$$

The master curve form of the Cross model for stress is as follows:

$$\frac{\sigma(\dot{\gamma}, P)}{a'_P(P)} = \frac{\eta_0(P_0)\dot{\gamma}}{1 + |\lambda(P_0)\dot{\gamma}a'_P(P)|^{m(P_0)}} \tag{48}$$

where $\eta_0(P_0)$, $m(P_0)$, and $\lambda(P_0)$ are the fitting parameters determined at $P_0$, 1 atm. The viscosity master curve version of the Cross model is:

$$\frac{\eta(\dot{\gamma})}{a'_P(P)} = \frac{\eta_0(P_0)}{1 + |\lambda(P_0)\dot{\gamma}a'_P(P)|^{m(P_0)}} \tag{49}$$

The resulting master curve and fitted Cross equation curve are shown in Figure 18. The zero-shear viscosity at $P$ is then calculated by:

$$\eta_0(P) = a'_P(P)\eta_0(P_0) \tag{50}$$

The shifted results show good superposition, and this implies that this material shows piezorheological simplicity, i.e., the pressure shift factor at each pressure is independent of shear rate. However, we will find that a vertical shift factor for concentration, $b_C$, is essential for the superposition of data for polymer with dissolved $CO_2$ due to the important effect of the gas on the melt density.

**8.3. Pressure Sensitivity of Viscosity.** To obtain the effect of pressure on the viscosity, the shift factor for pressure was determined. Figure 19 shows pressure shift factor versus pressure

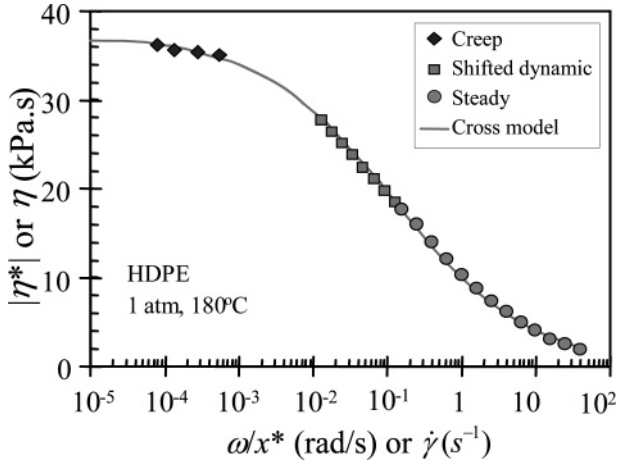


**Figure 16.** Cross model fitting. $\eta_0$ is 37.3 kPa·s, $\lambda$ is 8.2 $s^{-1}$, and $m$ is 0.48 at 180 °C and 1 atm.

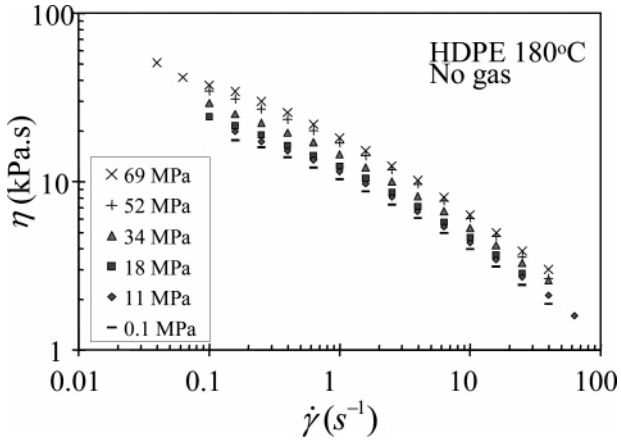


**Figure 17.** Effect of pressure on the viscosity vs shear rate curve.

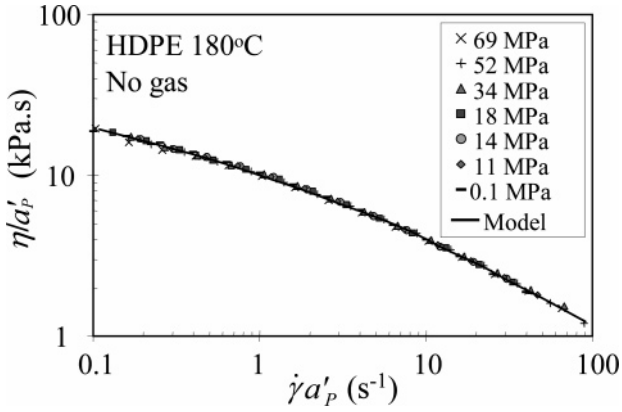


**Figure 18.** Shifted viscosity using $a'_P(P)$ and assuming $b_P$ to be one. $P_0 = 0.1$ MPa.

as well as the line fitted to the Barus model:[37]

$$\ln[a'_P(P)] = \beta(P - P_0) \tag{51}$$

where $\beta$ was found to be 15.2 $GPa^{-1}$.

**8.4. Combined Effects of Pressure and $CO_2$ on Viscosity.** Viscosity versus shear-rate data at five pressures under $CO_2$ at 180 °C are shown in Figure 20. Saturation was confirmed by the constancy of the viscosity with time. Data without $CO_2$ are also shown for comparison. Open symbols are for samples saturated with $CO_2$. While pressure alone increases the viscosity, pressure combined with $CO_2$ has the opposite effect even at a given pressure. This results from plasticization by the $CO_2$. For example, the data at 11 MPa are slightly higher than those at 1 atm, while these with $CO_2$ at 11 MPa are well below the atmospheric pressure points. The effect of $CO_2$ is clearly very large because it not only compensates for the increase of viscosity due to pressure but even decreases the viscosity below its value at atmospheric pressure. We note that increasing the $CO_2$ pressure from 46 to 52 MPa has negligible effect on the viscosity. This implies that the effect of increasing the pressure from 46 to 52 MPa is exactly balanced by the plasticization effect of the $CO_2$ and that the viscosity cannot be decreased further by increasing the $CO_2$ pressure above 46 MPa.

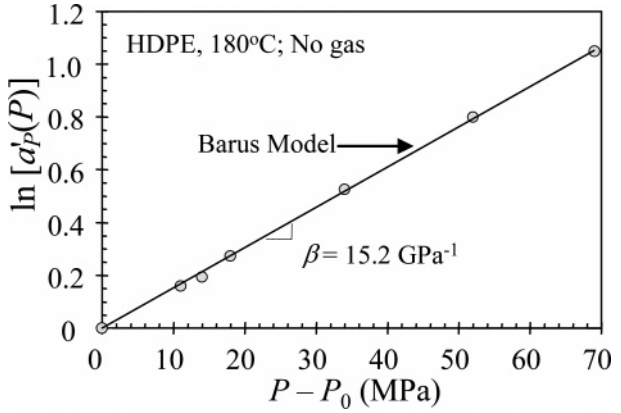


**Figure 19.** Effect of pressure on pressure shift factor, $P_0 = 0.1$ MPa.

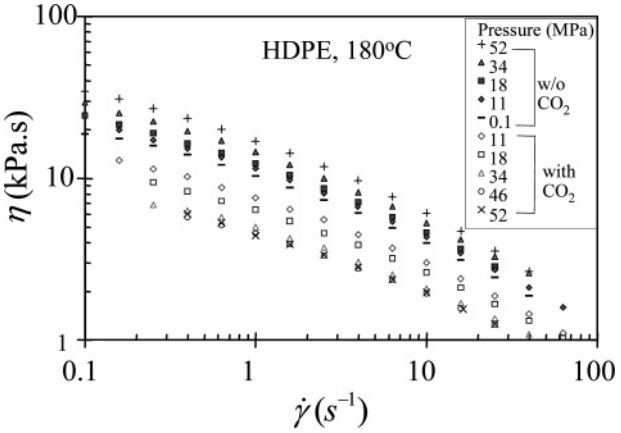


**Figure 20.** Effects of pressure and $CO_2$ on the viscosity vs shear rate curve.

The data were shifted to form a master curve. While the vertical shift for pressure was neglected, the vertical shift for concentration had to be taken into account, as it is a strong function of concentration. Figure 8 shows there is a 24% decrease over 34.5 MPa. Equation 52 defines this shift factor:

$$b_{P,C}(P, C) \equiv \frac{C_{pol}(P, C)}{\rho_{pol}(P_0, C_0)} \tag{52}$$

where $C_{pol}(P, C) \equiv W_{pol}/V_m(P, C)$, and $\rho_{pol}(P_0) \equiv W_{pol}/V_{pol}(P_0)$. To obtain pressure and concentration shift factor, the Cross model of stress was used. The master curve of the model with both horizontal and vertical shift factors is:

$$\frac{\sigma(\dot\gamma, P, C)}{a_{P,C}(P, C)b_C(C)} = \frac{\eta_0(P_0)\dot\gamma}{1 + |\lambda(P_0)\dot\gamma a_{P,C}(P, C)|^{m(P_0)}} \tag{53}$$

where $a_{P,C}(P, C)$ is the combined pressure and concentration shift factor assuming $b_{P,C}(P, C)$ equal to $b_C(C)$ due to the small effect of $P$ on density:

$$b_{P,C}(P, C) \cong b_C(C) \tag{54}$$

The viscosity master curve form of the Cross model with both horizontal and vertical shift factors is:

$$\frac{\eta(\dot\gamma, P, C)}{a_{P,C}(P, C)b_C(C)} = \frac{\eta_0(P_0)}{1 + |\lambda(P_0)\dot\gamma a_{P,C}(P, C)|^{m(P_0)}} \tag{55}$$

Figure 21 shows the resulting master curve. The shifted results show good superposition, and this implies that the horizontal and vertical pressure and concentration shift factors are independent of shear rate.

**8.5. Pressure and Concentration Sensitivity of Viscosity.** To describe the effects of pressure and concentration on viscosity, the dependencies of the shift factors on pressure and concentration were determined. Figure 22 shows the two shift factors as functions of pressure. As mentioned above, to study the effect of $CO_2$ at constant pressure, it is assumed that effects of pressure and $CO_2$ are separable, i.e., $a_{P,C}(P, C) = a'_P(P)$-$a_C(C)$:

$$\frac{\eta_0(P, C)}{\eta_0(P_0, C_0)} = a_{P,C}(P, C)b_C(C) = a'_P(P)a_C(C)b_C(C) \tag{56}$$

where $a'_P(P)$ is the shift factor assuming $b_P(P)$ to be one, and $a_C(C)$ is a horizontal concentration shift factor and is assumed to be related to $a_{P,C}(P, C)$ as follows:

$$a_C(C) = a_{P,C}(P, C)/a'_P(P) \tag{57}$$

The concentration shift factor $a_C(C)b_C(C)$ can thus be obtained as:

$$a_C(C)b_C(C) = a_{P,C}(P, C)b_C(C)/a'_P(P) \tag{58}$$

where all terms on the right-hand side are data. The quantity $a_C(C)b_C(C)$ represents a pressure-independent ratio of zero-shear viscosity at $C$ and $C_0$:

$$a_C(C)b_C(C) = \frac{\eta_0(C)}{\eta_0(C_0)} \tag{59}$$

where $C_0$ is zero for this study. The Fujita−Kishimoto (FK) model[38] (eq 24) for describing the effect of $CO_2$ concentration alone does not include $b_C$ explicitly. However, we included $b_C$ as shown by eq 60:

$$\ln\left[\frac{\eta_0(C)}{\eta_0(C_0)}\right] = \ln[a_C(C)b_C(C)] = \frac{-AC}{B + C} \tag{60}$$

where $C_0$ is zero, and $A$ and $B$ are fitting constants. Equation 60 can be rewritten to describe a straight line as follows:

$$\frac{1}{\ln[a_C(C)b_C(C)]} = -\frac{B}{A}\frac{1}{C} - \frac{1}{A} \tag{61}$$

According to eq 61, a plot of $1/\ln[a_C(C)b_C(C)]$ versus $1/C$ should be a straight line with a slope of $-B/A$ and an intercept of $-1/A$, and such a plot is shown in Figure 23. Figure 24 shows the two shift factors as functions of concentration along with the prediction of eq 60 with $A = 2.67$ and $B = 0.22$, as determined from Figure 23. We see that this model describes the effect of concentration fairly well. From this, we infer that $CO_2$ molecules increase the free volume of the polymer. In plastics processing, the polymer is generally not saturated, so for practical applications, independent shift factors for pressure and concentration are required.

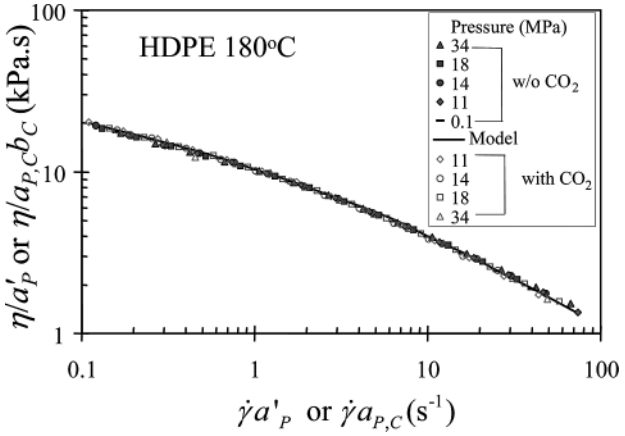


**Figure 21.** Viscosity shifted using both horizontal and vertical shift factors for $CO_2$ concentration. No vertical shift was used for the pure pressure effect.

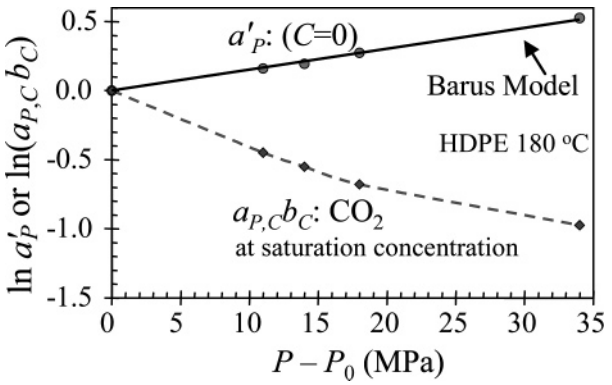


**Figure 22.** Shift factors as functions of pressure for $CO_2$.

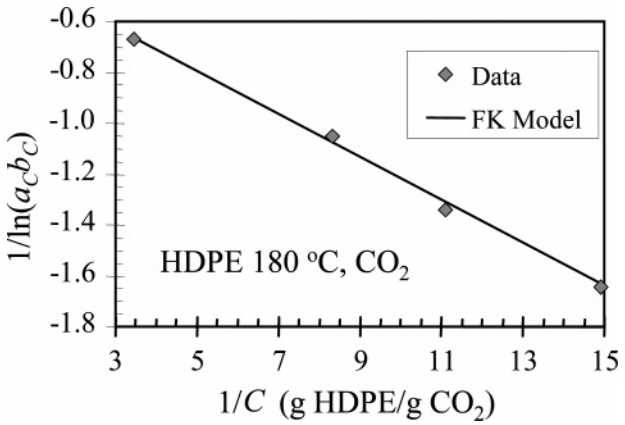


**Figure 23.** Effect of concentration on the concentration shift factor for $CO_2$. Line is best fit with $A = 2.67$ and $B = 0.22$.

**8.6. Comparison of Effects of $CO_2$ and $N_2$.** Figure 25 compares the effects of $CO_2$ and $N_2$ on viscosity at 34.5 MPa. The data for $N_2$ are the same as those at 1 atm, while those for $CO_2$ are well below the atmospheric data. The effect of $N_2$ is thus much less than that of $CO_2$ at the same pressure because the solubility of $N_2$ is only $^1/_7$ that of $CO_2$ (Tables 4 and 5).

It is of interest to compare effects of $N_2$ and $CO_2$ at the same concentration. For quantitative analysis of the comparison, the method of reduced variables was used. The vertical shift factor, $b_{P,C}(P, C)$ for $N_2$ was assumed to be unity because the available data are limited to low pressures and the solubility of $N_2$ is very low, and little swelling is expected (eq 21). A master curve

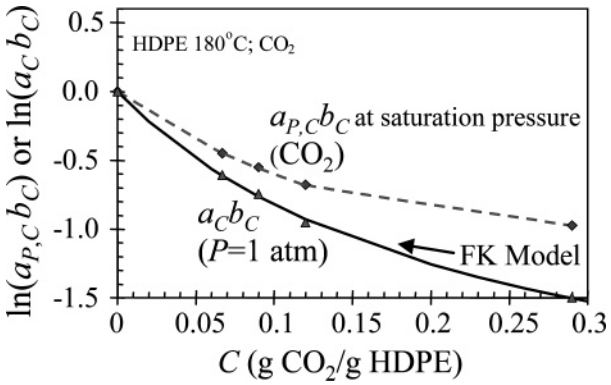


**Figure 24.** Shift factors as functions of concentration for $CO_2$.

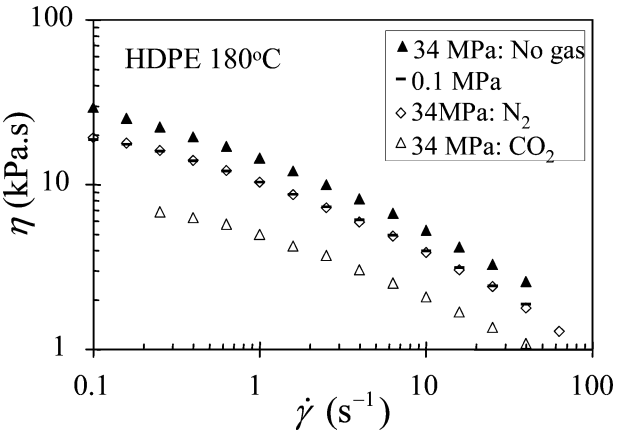


**Figure 25.** Comparison of the effects of $CO_2$ and $N_2$ on viscosity at 34 MPa.

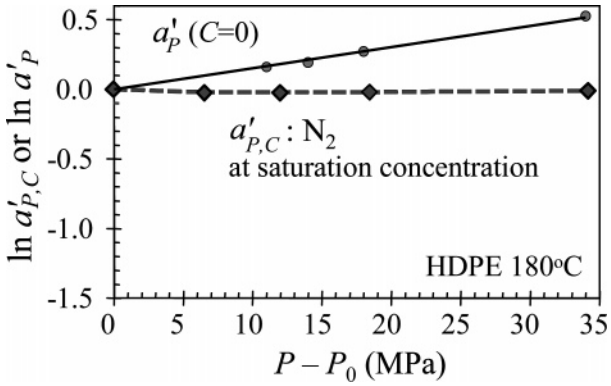


**Figure 26.** Shift factors as functions of pressure for $N_2$.

was built by determining $a'_{P,C}(P, C)$, the combined shift factor of pressure and concentration, assuming $b_{P,C}(P, C)$ to be unity:

$$\sigma(P, C) \text{ versus } \dot{\gamma}a'_{P,C}(P, C) \tag{62}$$

Figure 26 shows shift factors as functions of pressure. The values of $\ln[a'_{P,C}(P, C)]$ are very close to zero, and this implies that the viscosity of HDPE plasticized with $N_2$ at high pressures 6, 12, 18, and 34.5 MPa is similar to that at 1 atm. The increase of the viscosity due to pure pressure is exactly compensated by the plasticizing effect of $N_2$ at those pressures.

Because of the high solubility of $CO_2$, the effect of plasticization is larger than that of pressure alone, and this means that the $\ln(a_{P,C}b_C)$ is negative, i.e., that $|\ln(a_Cb_C)| > |\ln a'_P|$ at all pressures. This phenomenon resembles retrograde vitrification,[70−75] which is when the glass transition temperature $T_g$ decreases with $P$ in the presence of dissolved gas if both the solubility of the gas and the plasticization effect increase with pressure. This is the opposite of the effect of pressure alone, which is that $T_g$ increases with pressure. In the case of the system we studied, the measurement temperature of 180 °C was far above $T_g$ at 1 atm, which was −120 °C, and we would not expect a viscosity decrease to be related to $T_g$ depression. In the case of a polymer with a much higher $T_g$, such as polystyrene, this effect would have to be taken into account. However, at low solubility, $\ln(a_{P,C}b_C)$ may not be negative. For example, Figure 26 shows that this quantity ($\ln a'_{P,C}$ for $N_2$) is near to zero, and if a gas has a very low solubility, $\ln(a_{P,C}b_C)$ will be positive, i.e., that $|\ln(a_Cb_C)| < |\ln a'_P|$, and the viscosity with dissolved gas at high pressure will be higher than that at one atm. This can also happen with $CO_2$ because $\ln a'_P$ increases linearly with $P$, while the decrease of $\ln(a_Cb_C)$ is concave down, so that the second derivative of $\ln(a_Cb_C)$ is negative. This implies a minimum in the curve of $\ln(a_{P,C}b_C)$ versus $P$ that is like that in the curve of $T_g$ versus $P$ plot,[70,71] but in the experimental window where solubility data were available to us, $\ln(a_{P,C}b_C)$ only decreases, as shown in Figure 22.

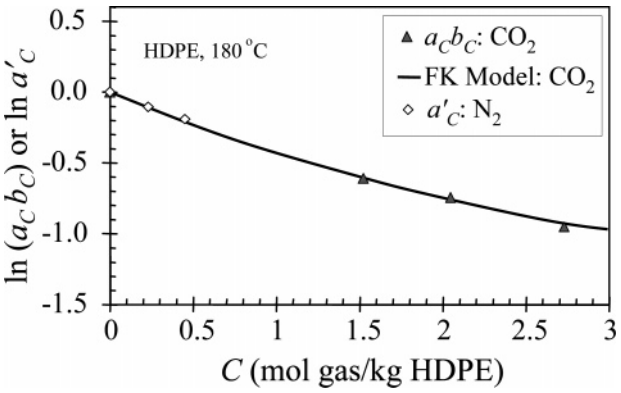


**Figure 27.** Comparison between shift factors for $CO_2$ and $N_2$.

The pressure-independent concentration shift factor for $N_2$ was calculated as:

$$a'_C(C) = a'_{P,C}(P, C)/a'_P(P) \tag{63}$$

Figure 27 shows shift factors for $CO_2$ and $N_2$ as functions of molar concentration. The solubility data of $N_2$ are limited, so that only the first three points in Figure 26 were used in Figure 27, but a trend can be seen. The FK model prediction for $CO_2$ describes the shift factor versus concentration data for $N_2$ very well, and the two gases have very similar effects on the viscosity at the same concentration expressed in moles. The same number of moles here does not imply the same volume because different pressures need to be applied to achieve the same concentration.

## 9. Conclusions

A high-pressure sliding plate rheometer was used to determine the effects of pressure and dissolved carbon dioxide on the viscosity of a high-density polyethylene (HDPE) at 180 °C, at pressures up to 70 MPa, and at concentrations up to 0.3 g $CO_2$/g HDPE. In this instrument, the pressure, gas concentration, temperature, and shear rate are all uniform. Because the gas of interest was the pressurizing fluid, all the data reported are for melt saturated with gas. However, by use of an inert oil, it was also possible to determine the effect of pressure alone at zero gas concentration. To interpret the data, it was necessary to know the *PVT* behavior of the melt both without gas and saturated with gas, as well as the solubility of the gas. A Gnomix *PVT* apparatus was used to determine the *PVT* behavior of pure

polymer, and the data were fitted to the Tait equation. A magnetic suspension balance was used to determine the solubility of the gas at each pressure and the swollen volume. The Sanchez−Lacombe equation was used to describe these data.

Fick's law was used to estimate the time required to effectively saturate a sample. For HDPE, the time is within practical limits, but for polystyrene, several days would be required. The stress measured at the center of the sample as a function of time was found to provide a sensitive indication of the degree of saturation. Small-amplitude oscillatory shear was found to significantly accelerate the diffusion of $CO_2$ in the sample.

The Cross model was found to fit the viscosity data quite well. The pure melt was found to exhibit time−pressure superposition, and the effect of pressure was well-described by the Barus equation. Assuming that the pressure shift factor could be combined with a concentration shift factor, it was shown that data at all pressures and concentrations could be brought together on a single master curve. An equation proposed by Fujita and Kishimoto was found to describe the effects of concentration on the concentration shift factor.

Carbon dioxide has a strong plasticizing effect and, at saturation, it more than compensates for the increase in viscosity due to pressure. At equal molar concentrations, $CO_2$ and $N_2$ have the same effect on viscosity, but $N_2$ is much less soluble in HDPE than $CO_2$ at the same pressure.

**Acknowledgment.** The HDPE resin was provided by Yoshito Sasaki of Japan Polyolefins Co. Prof. Musa R. Kamal and Nitin Borse at McGill University provided training and access to the *PVT* apparatus. Prof. Chul B. Park and Guangming Li at the University of Toronto provided training and access to the MSB instrument. This research was funded by the Natural Sciences and Engineering Research Council of Canada.

## A. Appendix: Mixing Rule for SL Model and Derivation of Chemical Potentials

The characteristic density of the mixture is:

$$\rho_m^* \equiv \frac{\rho_1^* \rho_2^*}{w_1\rho_2^* + w_2\rho_1^*} \tag{64}$$

where subscripts 1, 2, and *m* refer to the diffusing substance, polymer, and their mixture, respectively, $w_1$ and $w_2$ are the weight fractions, and $w_1 + w_2 = 1$. The characteristic pressure for a mixture is defined as:

$$P_m^* \equiv \phi_1{}^2 P_1^* + \phi_2{}^2 P_3^* + 2\phi_1\phi_2 P_{12}^* \tag{65}$$

where $\phi_1$ and $\phi_2$ are close-packed volume fractions defined as:

$$\phi_1 \equiv \frac{w_1}{\rho_1^*} \div \left(\frac{w_1}{\rho_1^*} + \frac{w_2}{\rho_2^*}\right) \tag{66}$$

$$\phi_2 \equiv \frac{w_2}{\rho_2^*} \div \left(\frac{w_1}{\rho_1^*} + \frac{w_2}{\rho_2^*}\right) = 1 - \phi_1 \tag{67}$$

and $P_{12}^*$ is defined as follows in terms of the interaction parameter, $K_{12}$:

$$P_{12}^* \equiv (1 - K_{12})\sqrt{P_1^* P_2^*} \tag{68}$$

The average close-packed mer volume is

$$v_m^* = \phi_1{}^0 v_1^* + \phi_2{}^0 v_2^* \tag{69}$$

where

$$\phi_1{}^0 \equiv \frac{\phi_1 P_1^*/T_1^*}{\phi_1 P_1^*/T_1^* + \phi_2 P_2^*/T_2^*} = \frac{\phi_1/v_1^*}{\phi_1/v_1^* + \phi_2/v_2^*} = \frac{w_1/(\rho_1^*\ v_2^*)}{w_1/(\rho_1^*\ v_1^*) + w_2/(\rho_2^*\ v_2^*)} \tag{70}$$

and

$$\phi_2{}^0 = 1 - \phi_1{}^0 \tag{71}$$

The characteristic temperature for the mixture is:

$$T_m^* \equiv P_m^*\ v_m^*/R \tag{72}$$

The number of lattice sites[76] occupied by an *r*-mer is:

$$\frac{1}{r_m} \equiv \frac{\phi_1{}^0}{r_1} + \frac{\phi_2{}^0}{r_2} \tag{73}$$

There are three unknowns in the EOS for a binary mixture: $K_{12}$-$(T, P)$, $\rho_m(T, P)$, which is related to swollen volume, and $\phi_1(T, P)$, which is related to the solubility.

At equilibrium, the chemical potential of component 1 in gas phase and that in polymer are the same:

$$\mu_1{}^1 = \mu_1^m \tag{74}$$

Sanchez and Lacombe[45] derived an expression for the Gibbs free energy of a binary mixture:

$$G_m = r_m N_m \epsilon_m^* \left\{\tilde{T}_m\left[\frac{\phi_1}{r_1}\ln\phi_1 + \frac{\phi_2}{r_2}\ln\phi_2\right] - \tilde{\rho}_m + \frac{\tilde{P}_m}{\tilde{\rho}_m}\right\} + r_m N_m \epsilon_m^* \frac{\tilde{T}_m}{\tilde{\rho}_m}\left[(1-\tilde{\rho}_m)\ln(1-\tilde{\rho}_m) + \frac{\tilde{\rho}_m}{r_m}\ln\tilde{\rho}_m\right] \tag{75}$$

The chemical potential of component 1 in the mixture can be obtained by differentiating the Gibbs free energy with respect to the number of molecules of component 1, $N_1$:

$$\mu_1^m = \left(\frac{\partial G_m}{\partial N_1}\right)_{T,P,N_2} \tag{76}$$

Sanchez and Lacombe[45] derived $\mu_1^m$ as:

$$\mu_1^m = RT\left[\ln\phi_1 + \left(1 - \frac{r_1}{r_2}\right)\phi_2 + r_1{}^0\tilde{\rho}_m\frac{P_1^* + P_2^* - 2P_{12}^*}{P_1^*\tilde{T}_1}\phi_2{}^2\right] + r_1{}^0 RT\left[-\frac{\tilde{\rho}_m}{\tilde{T}_1} + \frac{\tilde{P}_1}{\tilde{\rho}_m\tilde{T}_1} + \left(\frac{1}{\tilde{\rho}_m} - 1\right)\ln(1-\tilde{\rho}_m) + \frac{1}{r_1{}^0}\ln\tilde{\rho}_m\right] \tag{77}$$

where $\tilde{P}_1 \equiv P/P_1^*$, $\tilde{T}_1 \equiv T/T_1^*$, and two new parameters are defined for simplification:

$$r_1^0 \equiv \frac{M_1 P_1^*}{R T_1^* \rho_1^*} \tag{78}$$

$$r_2^0 \equiv \frac{M_2 P_2^*}{R P_2^* \rho_2^*} \tag{79}$$

The chemical potential of component 1 in a pure phase can be obtained from eq 77 by replacing $\tilde{\rho}_m$ with $\tilde{\rho}_1$ and letting $\phi_1 = 1$ and $\phi_2 = 0$:

$$\mu_1^1 = r_1^0 RT\left[-\frac{\tilde{\rho}_1}{\tilde{T}_1} + \frac{\tilde{P}_1}{\tilde{\rho}_1 \tilde{T}_1} + \left(\frac{1}{\tilde{\rho}_1} - 1\right)\ln(1-\tilde{\rho}_1) + \frac{1}{r_1^0}\ln\tilde{\rho}_1\right] \tag{80}$$

where $\tilde{\rho}_1 \equiv \rho_1/\rho_1^*$, and eq 74 can be expressed as:

$$r_1^0 RT\left[-\frac{\tilde{\rho}_1}{\tilde{T}_1} + \frac{\tilde{P}_1}{\tilde{\rho}_1 \tilde{T}_1} + \left(\frac{1}{\tilde{\rho}_1} - 1\right)\ln(1-\tilde{\rho}_1) + \frac{1}{r_1^0}\ln\tilde{\rho}_1\right]$$
$$= RT\left[\ln\phi_1 + \left(1 - \frac{r_1}{r_2}\right)\phi_2 + r_1^0\tilde{\rho}_m\frac{P_1^* + P_2^* - 2P_{12}^*}{P_1^*\tilde{T}_1}\phi_2^2\right] +$$
$$r_1^0 RT\left[-\frac{\tilde{\rho}_m}{\tilde{T}_1} + \frac{\tilde{P}_1}{\tilde{\rho}_m \tilde{T}_1} + \left(\frac{1}{\tilde{\rho}_m} - 1\right)\ln(1-\tilde{\rho}_m) + \frac{1}{r_1^0}\ln\tilde{\rho}_m\right] \tag{81}$$

## References and Notes


(1) Penninger, J. M. L.; Radosz, M.; McHug, M. A.; Krukonis, V. J.; *Supercritical Fluid Technology*; Elsevier: Amsterdam, 1985.
(2) Johnston, K. P.; Penninger, J. M. L. *Supercritical Fluid Science and Technology*; American Chemical Society: Washington, DC, 1989.
(3) Dean, J. R. *Applications of Supercritical Fluids in Industrial Analysis*; Blackie Academic & Professional: London, 1993.
(4) De Castro, M. D. L.; Valcácel, M.; Tena, M. T. *Analytical Supercritical Fluid Extraction*; Springer-Verlag: Berlin, 1994.
(5) McHugh, M. A.; Krukonis, V. J. *Supercritical Fluid Extraction*, 2nd ed.; Elsevier: Amsterdam, 1994.
(6) Taylor, L. T. *Supercritical Fluid Extraction*; John Wiley & Sons: New York, 1996.
(7) McHardy, J.; Sawan, S. P. *Supercritical Fluid Cleaning*; Noyes Publications: Westwood, NJ, 1998.
(8) Clifford, T. *Fundamentals of Supercritical Fluids*; Oxford University Press: Oxford, 1999.
(9) DeSimone, J. M. *Science* **2002**, *297*, 799−803.
(10) DeSimone, J. M.; Tumas, W. *Green Chemistry Using Liquid and Supercritical Carbon Dioxide*; Oxford University Press: Oxford, 2003.
(11) Tomasko, D. L.; Li, H.; Liu, D.; Han, X.; Wingert, M. J.; Lee, L. J.; Koelling, K. W. *Ind. Eng. Chem. Res.* **2003**, *42*, 6431−6456.
(12) DeSimone, J. M.; Guan, Z.; Elsbernd, C. S. *Science* **1992**, *257*, 945−947.
(13) Landrock, A. H. *Handbook of Plastic Foams*; Noyes Publications: Park Ridge, NJ, 1995.
(14) Khemani, K. C. *Polymeric Foams*; American Chemical Society: Washington, DC, 1997.
(15) Okamoto, K. T. *Microcellular Processing*; Hanser: Munich, 2003.
(16) Wall, L. In *High Polymers Series*; Wiley-Interscience: New York, 1972; Vol. 25.
(17) Collins, W. J.; Derwent, R. G.; Johnson, C. E.; Stevenson, D. S. *Clim. Change* **2002**, *52*, 453−479.
(18) Solomon, S.; Garcia, R. R.; Rowland, F. S..; Wuebbles, D. J. *Nature* **1986**, *321*, 755−758.
(19) Parson, E. A. *Protecting the Ozone Layer*; Oxford University Press: Oxford, 2003.
(20) Houghton, J. T.; Filho, L. G. M.; Callander, B. A.; Harris, N.; Kattenberg, A.; Maskell, K. *Climate Change 1995*: *The Science of Climate Change*; Cambridge University Press: Cambridge, 1996.
(21) Gerhardt, L. J.; Manke, C. W.; Gulary, E. *J. Polym. Sci., Part B: Polym. Phys*. **1997**, *35*, 523−534.
(22) Gerhardt, L. J.; Garg, A.; Manke, C. W.; Gulary, E. *J. Polym. Sci., Part B: Polym. Phys*. **1998**, *33*, 1911−1918.
(23) Kwag, C.; Manke, C. W.; Gulari, E. *J. Polym. Sci., Part B: Polym. Phys*. **1999**, *37*, 2771−2781.
(24) Kwag, C.; Manke, C. W.; Gulari, E. *Ind. Eng. Chem. Res*. **2001**, *40*, 3048−3052.
(25) Lee, M. H.; Tzoganakis, C.; Park, C. B. *Polym. Eng. Sci*. **1998**, *28*, 1112−1120.
(26) Lee, M. H.; Park, C. B.; Tzoganakis, C. *Polym. Eng. Sci*. **1999**, *39*, 99−109.
(27) Ladin, D.; Park, C. B.; Park, S. S.; Naguib, H. E.; Cha, S. W. *J. Cell. Plast.* **2001**, *37*, 109−148.
(28) Royer, J. R.; Gay, Y. J.; Desimone, J. M.; Khan, S. A. *J. Polym. Sci., Part B: Polym. Phys*. **2000**, *28*, 3168−3180.
(29) Chow, T. *Macromolecules* **1980**, *13*, 362−364.
(30) Utracki, L. A.; Simha, R. *J. Polym. Sci., Part B: Polym. Phys.* **2001**, *39*, 342−362.
(31) Yeo, S.-D.; Kiran, E. *Macromolecules* **1999**, *32*, 7325−7328.
(32) Yeo, S.-D.; Kiran, E. *J. Appl. Polym. Sci.* **2000**, *75*, 306−315.
(33) Oh, J.-H.; Lindt, J. T. *60th Annu. Tech. Conf.—Soc. Plast. Eng.* **2002**, *2*, 1920−1923.
(34) Ferry, J. D. *J. Am. Chem. Soc*. **1950**, *72*, 3746−3752.
(35) Rouse, P. E., Jr. *J. Chem. Phys.* **1953**, *21*, 1272−1280.
(36) Plazek, D. J. *J. Rheol.* **1996**, *40*, 987−1014.
(37) Barus, C. *Am. J. Sci.* **1883**, *45*, 87−96.
(38) Fujita H.; Kishimoto, A. *J. Polym. Sci.* **1958**, *28*, 547−567.
(39) Williams, M. L.; Landel, R. F.; Ferry, J. D. *J. Am. Chem. Soc*. **1955**, *77*, 3701−3707.
(40) Sato, Y.; Fujiwara, K.; Takikawa, T.; Sumarno; Takishima, S.; Masuoka, H. *Fluid Phase Equilib*. **1999**, *162*, 261−276.
(41) Tait, P. G. In *Report on the Scientific Results of the Voyage of H.M.S. Challenger during the Years* 1873−1876: *Physics and Chemistry*; H.M. Stationery Office: London, 1888; Vol. 2, Part IV, pp 1−68.
(42) Wohl, A. *Z. Phys. Chem.* **1921**, *99*, 234−241.
(43) Cutler, W. G.; McMickle, R. H.; Webb, W.; Schiessler, R. W. *J. Chem. Phys*. **1958**, *29*, 727−740.
(44) Sanchez, I. C.; Lacombe, R. H. *J. Phys. Chem.* **1976**, *80*, 2352−2362.
(45) Sanchez, I. C.; Lacombe, R. H. *Macromolecules* **1978**, *11*, 1145−1156.
(46) Li, G.; Wang, J.; Park, C. B.; Moulinie, P.; Simha, R. *62nd Annu. Tech. Conf.—Soc. Plast. Eng.* **2004**, *2*, 2566−2575.
(47) Funami, E.; Taki, K.; Kihara, S.; Ohshima, M. 10th APCChE, Kitakyushu, Japan, 2004, Section 2H-10.
(48) Zoller, P.; Bolli, P.; Pahud, V.; Ackermann, H. *Rev. Sci. Instrum.* **1976**, *47*, 948−952.
(49) Capt, L.; Kamal, M. R. *Int. Polym. Process.* **2000**, *15*, 83−94.
(50) Rodgers, P. A. *J. Appl. Polym. Sci.* **1993**, *48*, 1061−1080.
(51) Hilic, S.; Boyer, S. A. E.; Padua, A. A. H.; Grolier; J. P. E. *J. Polym. Sci., Polym. Phys*. **2001**, *39*, 2063−2070.
(52) Kiszak, M. B.; Meilchen, M. A.; McHugh, M. A. *J. Appl. Polym. Sci*. **1998**, *36*, 583−597.
(53) Sato, Y.; Takikawa, T.; Sorakubo, A.; Takishima, S.; Masuoka, H. *Ind. Eng. Chem. Res.* **2000**, *39*, 4813−4819.
(54) Sato, Y.; Takikawa, T.; Takishima, S.; Masuoka, H. *J. Supercrit. Fluids* **2001**, *19*, 187−198.
(55) Park, H. E. Effects of Pressure and Dissolved Carbon Dioxide on the Rheological Properties of Molten Polymers. Doctoral Thesis, McGill University, Montreal, 2005.
(56) Areerat, S.; Hayata, Y.; Katsumoto, R.; Kegasawa, T.; Egami, H.; Ohshima, M. *J. Appl. Polum. Sci*. **2002**, *86*, 282−288.
(57) Fick, A. *Ann. Phys. Chem.* **1855**, *94*, 59−86.
(58) Carslaw, H. S.; Jaeger, J. C. *Conduction of Heat in Solids*, 2nd ed.; Clarendon Press: Oxford, 1959; p 33.
(59) Crank, J. *The Mathematics of Diffusion*, 2nd ed.; Clarendon Press: Oxford, 1975; p 47.
(60) Giacomin, A. J. A Sliding Plate Melt Rheometer Incorporating a Shear Stress Transducer. Doctoral Thesis, McGill University, Montreal, 1987.
(61) Giacomin, A. J.; Samurkas, T.; Dealy, J. M. *Polym. Eng. Sci.* **1989**, *29*, 499.
(62) Koran, F. The Effect of Pressure on the Rheology and Wall Slip of Polymer Melts. Doctoral Thesis, McGill University, Montreal, 1998.
(63) Koran, F.; Dealy, J. M. *J. Rheol.* **1999**, *43*, 1279−1290.
(64) Cox, W. P.; Merz, E. H. *J. Polym. Sci.* **1958**, *28*, 619−622.
(65) Rabinowitsch, B. *Z. Phys. Chem.* **1929**, *145*, 1−26.
(66) Chmiel, H.; Schümmer, P. *Chem.-Ing.-Tech.* **1971**, *43*, 1257−1259.
(67) Schümmer, P.; Worthoff, R. H. *Chem. Eng. Sci.* **1978**, *33*, 759−763.
(68) Dealy, J. M.; Wissbrun, K. F. *Melt Rheology and Its Role in Plastics Processing*; Chapman and Hall: London, 1995; p 303.
(69) Cross, M. M. In *Polymer Systems: Deformation and Flow*: Proceedings of the 1966 Annual Conference of the British Society of Rheology;

Wetton, R. E., Whorlow; R. W., Eds.; MacMillan: London, 1968; pp 263−273.
(70) Wang, W.-C. V.; Kramer, E. J.; Sachse, W. H. *J. Polym. Sci., Polym. Phys. Ed.* **1982**, *20*, 1371−1384.
(71) Condo, P. D.; Sanchez, I. C.; Panayiotou, C. G.; Johnston, K. P. *Macromolecules* **1992**, *25*, 6119−6127.
(72) Condo, P. D.; Johnston, K. P. *Macromolecules* **1992**, *25*, 6730−6732.
(73) Di Marzio, E. A.; Castellano, C.; Yang, A. *J. Polym. Sci., Part B*: *Polym. Phys.* **1996**, *34*, 535−543.
(74) Handa, Y. P.; Zhang, Z. *J. Polym. Sci., Part B: Polym. Phys.* **2000**, *38*, 716−725.
(75) Pham, J. Q.; Johnston, K. P.; Green, P. F. *J. Phys. Chem. B* **2004**, *108*, 3457−3461.
(76) Orbey, H.; Bokis, C. P.; Chen, C.-C. *Ind. Eng. Chem. Res.* **1998**, *37*, 4481−4491.

MA060735+